Magnetization of rotating ferrofluids: the effect of polydispersity

2006 J. Phys.: Condens. Matter 18 S2633

(http://iopscience.iop.org/0953-8984/18/38/S07)

INSTITUTE OF PHYSICS PUBLISHING JOURNAL OF PHYSICS: CONDENSED MATTER

J. Phys.: Condens. Matter **18** (2006) S2633–S2642 doi:10.1088/0953-8984/18/38/S07

Magnetization of rotating ferrofluids: the effect of polydispersity

A Leschhorn, J P Embs and M Lücke

Institut für Theoretische Physik, Universität des Saarlandes, D-66041 Saarbrücken, Germany

Received 15 May 2006
Published 8 September 2006
Online at stacks.iop.org/JPhysCM/18/S2633

Abstract

The influence of polydispersity on the magnetization is analysed in a non-equilibrium situation where a cylindrical ferrofluid column is forced to rotate with constant frequency, like a rigid body in a homogeneous magnetic field that is applied perpendicular to the cylinder axis. Then, the magnetization and the internal magnetic field are no longer parallel to each other and their directions differ from that of the applied magnetic field. Experimental results on the transverse magnetization component perpendicular to the applied field are compared and analysed as functions of rotation frequency and field strength with different polydisperse Debye models that take into account the polydispersity in different ways and to a varying degree.

1. Introduction

The prospect of influencing the rotational dynamics of nanoscale magnetic particles in a ferrofluid by a macroscopic flow and/or by a magnetic field in order to then observe the resulting response via the magnetization and/or via changes in the flow has been stimulating many research activities [1–4] ever since McTague measured [5] the so-called magneto-viscous effect. Of particular interest in this context are flows that are shear free on the macroscopic scale, as in a fluid that is rotating like a rigid body with a rotation frequency, say, $\mathbf{\Omega} = \Omega \mathbf{e}_z$.

While the colloidal magnetic particles then undergo thermally sustained rotational and translational Brownian motion on the microscopic scale, they co-rotate on average with the deterministic macroscopic rigid body flow. However, this mean co-rotation can be hindered by magnetic torques on their moments when a magnetic field, say, $\mathbf{H}_0 = H_0 \mathbf{e}_x$, is applied perpendicular to the rotation axis $\mathbf{e}_z$ of the flow. The combination of the externally imposed forcing of the particle motion by (i) the rigid body flow in which they are floating and by (ii) the magnetic torques on their magnetic moments drives the colloidal suspension out of equilibrium. Concerning the magnetic moments, this forcing causes the mean orientation of the moments, i.e. of the magnetization $\mathbf{M}$ of the ferrofluid, to be no longer parallel to the internal magnetic field $\mathbf{H}$. Instead, $\mathbf{M}$ is pushed out of the direction of $\mathbf{H}$ as well as of that of $\mathbf{H}_0$, thereby acquiring a non-zero transverse component M_y. Here it should be noted that, in a long

cylinder, Maxwell's equations imply the vector relation $\mathbf{H} = \mathbf{H}_0 - \mathbf{M}/2$ between the three fields when they are stationary and homogeneous, but they do not need to be collinear. However, in equilibrium, $\boldsymbol{\Omega} = 0$, the three fields are indeed collinear: the equilibrium magnetization $\mathbf{M}_{\mathrm{eq}}(\mathbf{H}) = M_{\mathrm{eq}}(H)\mathbf{H}/H$ is parallel to the internal field $\mathbf{H}$.

Recently, the transverse magnetization M_y of a slender cylindrical column of ferrofluid that was forced to rotate like a rigid body with constant frequency $\Omega\mathbf{e}_z$ in an applied homogeneous magnetic field $H_0\mathbf{e}_x$ was measured as a function of Ω and H_0 [6]. These measurements showed, among others, that the predictions [7] based on models for the magnetization dynamics [8–12] with a single relaxation time overestimate the magnitude of M_y. One reason for this discrepancy seems to be that particles with different sizes and different rotational dynamics of their magnetic moments contribute differently to the non-equilibrium, flow-induced component M_y of the magnetization. In particular, only the magnetic moments of the larger particles in which the magnetic moments are blocked and 'frozen' in the particles, i.e. those with effective Brownian relaxation dynamics, may be rotated by the flow out of the direction of the magnetic field.

Here we consider polydisperse models with single-particle Brownian as well as Néel relaxation dynamics for different particle sizes. So we ignore the influence of any dipolar magnetic interaction and of any flow-induced interaction on the (rotation) dynamics of the particles. Thereby collective, collision-dominated long-range and long-time hydrodynamic relaxation dynamics of the ensemble of magnetic moments are discarded, since only the individual relaxation of each magnetic moment is considered—albeit in the collectively generated internal magnetic field $\mathbf{H}$.

2. Equilibrium magnetization

In our experiments we used several ferrofluids from the APG-series of FerroTec. Their saturation magnetization was specified by the manufacturer to be $M_{\mathrm{sat}}^{\mathrm{FF}} = 17\,507$ A m^{-1} ($\pm 10\%$). This corresponds to a volume concentration $\phi \approx 3.6\%$ of the suspended magnetic material. We have measured the equilibrium magnetization of the ferrofluids with a vibrating sample magnetometer (LakeShore 7300 VSM) with a commercial PC user package. In order to get information on the particle size distribution of the ferrofluid under investigation, we used fits [13] with a log-normal form of the distribution as well as with a regularization procedure [6] based on Tichonovs method [14]. Generally, the equilibrium magnetization $M^{\mathrm{eq}}(H)$ as a function of the internal magnetic field H can be approximated by a superposition of Langevin functions:

$$M^{\mathrm{eq}}(H) = \sum_j w_j \mathcal{L}[\alpha_j(H)]. \tag{2.1}$$

Here $\mathcal{L}(x) = \coth(x) - 1/x$ denotes the Langevin function that depends on the dimensionless Langevin parameter $\alpha_j(H) = \mu_0 m_j H/k_{\mathrm{B}}T$, and w_j are the so-called magnetic weights. m_j refers to the magnetic moment of particles with magnetic diameter d_j, i.e. $m_j = \frac{\pi}{6} d_j^3 M_{\mathrm{sat}}^{\mathrm{bulk}}$, with $M_{\mathrm{sat}}^{\mathrm{bulk}}$ being the bulk-saturation magnetization. From equation (2.1) we can deduce the initial susceptibility $\chi_0 = \frac{\pi \mu_0 M_{\mathrm{sat}}^{\mathrm{bulk}}}{18 k_{\mathrm{B}} T} \sum_j w_j d_j^3$ and the saturation magnetization $M_{\mathrm{sat}}^{\mathrm{FF}} = \sum_j w_j$ of the ferrofluid under investigation.

Figure 1 shows the experimentally determined equilibrium magnetization $M_{\mathrm{eq}}(H)$ of APG 933 versus the internal field H together with fits that were obtained with a log-normal distribution [13] and with the regularization method [6]. The saturation magnetization of the ferrofluid sample was $M_{\mathrm{sat}}^{\mathrm{FF}} = 19\,108.6$ A m^{-1}. From the saturation magnetization, the volume concentration of the magnetite particles was found to be $\phi = M_{\mathrm{sat}}^{\mathrm{FF}}/M_{\mathrm{sat}}^{\mathrm{bulk}} = 4.1\%$, which is in

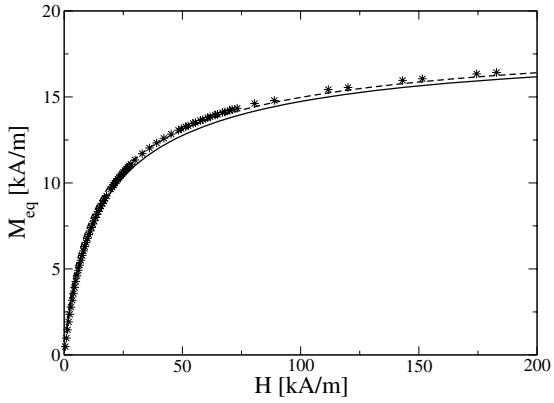

Figure 1. Equilibrium magnetization versus internal magnetic field for the ferrofluid AGP 933 of FerroTec. Symbols denote experimental data: solid line fit with a log-normal distribution, and dashed line fit with a regularization method. See text for further information.

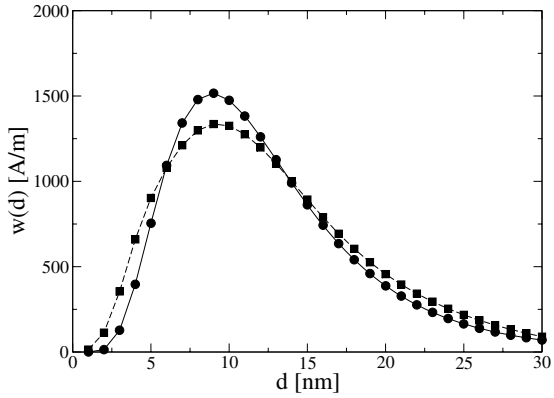

Figure 2. Magnetic weights of the 30 particle sizes considered here ($d_1 = 1$ nm to $d_{30} = 30$ nm) obtained from measurements of $M_{\mathrm{eq}}(H)$ in figure 1 by using a log-normal distribution (solid line, circles) and by using a regularization method (dashed line, squares).

reasonable agreement with the manufacturer's specifications. For the initial susceptibility we found the value $\chi_0 = 1.09$.

The magnetic weight distributions $w(d)$ resulting from the two fit methods are shown in figure 2.

3. Experimental setup

The experimental setup for measuring the magnetization of a rotating cylindrical column of a ferrofluid is sketched in figure 3. It is described in more detail in [6]. The ferrofluid is filled into a cylindrical plexiglass sample holder with an inside radius of $R = 3.2$ mm. This radius is so small that, for our rotation frequencies, the ferrofluid rotates as a rigid body with a flow field $\mathbf{u}(\mathbf{r}) = \boldsymbol{\Omega} \times \mathbf{r} = \Omega r \mathbf{e}_\varphi$. Here Ω is the externally forced constant rotation rate of the sample and $\mathbf{e}_\varphi$ is the unit vector in the azimuthal direction. A homogeneous and temporally constant magnetic field $\mathbf{H}_0 = H_0 \mathbf{e}_x$ is applied perpendicular to the cylinder axis $\mathbf{e}_z$. For such

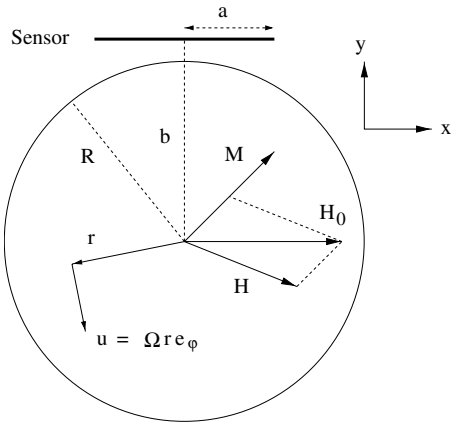

Figure 3. Schematic plot of the system. The cylindrical sample holder with inner radius R rotates with angular velocity $\boldsymbol{\Omega}$ in the applied static magnetic field $\mathbf{H}_0$ perpendicular to $\boldsymbol{\Omega}$. The magnetization M_y is measured with a Hall sensor. $\mathbf{M}$ and $\mathbf{H}$ denote the magnetization and internal magnetic field of the ferrofluid. Both are constant in space and time.

a combination of forced rotation and applied field, theoretical models allow for a spatially and temporally constant non-equilibrium magnetization $\mathbf{M}$ that is pushed out of the directions of $\mathbf{H}_0$ and $\mathbf{H}$ by the flow.

According to the Maxwell equations, the fields $\mathbf{H}$ and $\mathbf{M}$ within the ferrofluid are related to each other via

$$\mathbf{H} = \mathbf{H}_0 - \tfrac{1}{2}\mathbf{M} \tag{3.1}$$

for our long cylindrical sample and in particular $H_y = -M_y/2$, as indicated schematically in figure 3. In addition, they demand that the magnetic field outside the ferrofluid cylinder

$$\mathbf{H}^{\text{out}} = \mathbf{H}_0 + \frac{1}{2}\frac{R^2}{r^2}\left(2\frac{\mathbf{r}}{r}\frac{\mathbf{M}\cdot\mathbf{r}}{r} - \mathbf{M}\right) \tag{3.2}$$

is a superposition of the applied field $\mathbf{H}_0$ and the dipolar contribution from $\mathbf{M}$. This result yields a relation between the perpendicular component of the magnetization M_y (resp. of the internal field $H_y = -M_y/2$) and the field H_y^{sensor} measured by the Hall sensor outside the sample, as indicated in figure 3. Considering the finite size of the Hall sensor, H_y^{sensor} is given by

$$H_y^{\text{sensor}} = \frac{1}{2a}\int_{-a}^{a} H_y^{\text{out}}\,\mathrm{d}x = -\frac{R^2}{a^2+b^2}H_y. \tag{3.3}$$

In our experimental setup, $b = 4.75$ mm, $R = 3.2$ mm, and $a = 2$ mm; here a denotes the horizontal extension of the Hall sensor. So, $H_y^{\text{sensor}} = -0.386\,H_y$, where $H_y = -M_y/2$ is the y-component of the internal magnetic field in the ferrofluid.

4. Magnetization dynamics of a polydisperse model

Comparisons with experimental results showed [6] that theoretical predictions [7] based on models [8–12] with a single relaxation time overestimate the magnitude of H_y^{sensor}. One reason is that particles with different sizes and different rotational dynamics of their magnetic moments contribute differently to the non-equilibrium, flow-induced component M_y of the magnetization and that, in particular, only the magnetic moments of the larger particles with

effective Brownian relaxation dynamics may be rotated by the flow out of the direction of the magnetic field.

Therefore, here we consider as a next step polydisperse models with single-particle Brownian and Néel relaxation dynamics for different particle sizes. Such models have been used [15] to determine, within a linear response analysis, the effect of polydispersity on the dynamics of a torsional ferrofluid pendulum that was periodically forced close to resonance to undergo small amplitude oscillations in a rigid body flow [16, 17].

We ignore the influence of any dipolar magnetic interaction and of any flow-induced interaction on the (rotation) dynamics of the particles. Thereby collective, collision-dominated long-range and long-time hydrodynamic relaxation dynamics of the ensemble of magnetic moments are discarded, since only the individual relaxation of each magnetic moment is considered—albeit in the collectively generated internal magnetic field $\mathbf{H}$.

For numerical reasons, we use a discrete partition of the particle size distribution. Then, without interaction, the magnetization of the resulting mixture of mono-disperse ideal paramagnetic gases is given by $\mathbf{M} = \sum \mathbf{M}_j$, where $\mathbf{M}_j$ denotes the magnetization of the particles with diameter d_j. We assume that each magnetic moment, and with it each $\mathbf{M}_j$, obeys a simple Debye relaxation dynamics that drives them in the absence of flow towards their respective equilibrium value $\mathbf{M}_j^{\mathrm{eq}}(\mathbf{H})$. Then, in the stationary situation resulting from the rigid body rotation with constant $\boldsymbol{\Omega}$, the Debye relaxation equation for each sub-magnetization is given by

$$\boldsymbol{\Omega} \times \mathbf{M}_j = \frac{1}{\tau_j}[\mathbf{M}_j - \mathbf{M}_j^{\mathrm{eq}}(\mathbf{H})]. \tag{4.1}$$

In the absence of interactions, the equilibrium magnetization of each species is determined by a Langevin function

$$\mathbf{M}_j^{\mathrm{eq}}(\mathbf{H}) = \chi_j(H)\mathbf{H} = w_j \mathcal{L}\left(\frac{\mu_0 \pi M_{\mathrm{sat}}^{\mathrm{bulk}}}{6k_{\mathrm{B}}T} d_j^3 H\right)\frac{\mathbf{H}}{H}. \tag{4.2}$$

Here $M_{\mathrm{sat}}^{\mathrm{bulk}}$ is the bulk-saturation magnetization of the magnetic material. For the magnetic weight $w_j(d_j)$ of species j, we take the experimentally determined values in the representation (2.1).

We should like to draw the attention of the reader to the fact that the magnetization equations (4.1) for different particle sizes are coupled via the internal field $\mathbf{H}$: according to Maxwell's equations, $\mathbf{H} = \mathbf{H}_0 - \frac{1}{2}\mathbf{M}$ is given in terms of the total $\mathbf{M} = \sum \mathbf{M}_j$.

In the relaxation rate $1/\tau_j$ we take into account Brownian and Néel relaxation processes by adding their rates with equal weight

$$\frac{1}{\tau_j} = \frac{1}{\tau_{\mathrm{B}}^j} + \frac{1}{\tau_N^j}. \tag{4.3}$$

The relaxation times depend on the particle size according to $\tau_{\mathrm{B}}^j = \frac{\pi\eta}{2k_{\mathrm{B}}T}(d_j + 2s)^3$ and $\tau_N^j = f_0^{-1}\exp(\frac{\pi K d_j^3}{6k_{\mathrm{B}}T})$. Here, η is the viscosity, s is the thickness of the non-magnetic particle layer, and K is the anisotropy constant. The combined relaxation rate (4.3) is dominated by the faster of the two processes. Thus, large particles relax in a Brownian manner with relaxation times of about some 10^{-3} s, while small particles have much smaller Néel relaxation times. The boundary between Néel-and Brownian-dominated relaxation as a function of particle size d depends sensitively on the anisotropy constant K. This is documented in figure 4 for the two values $K = 15$ and $K = 50$ kJ m^{-3}. For these specific examples, the boundaries between Néel-and Brownian-dominated relaxation lie at about $d \simeq 20$ nm and $d \simeq 13$ nm, respectively.

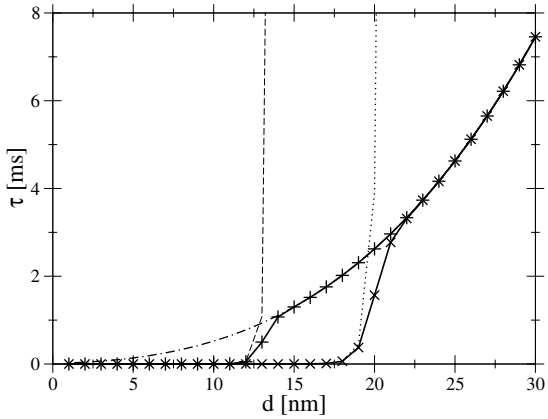

Figure 4. Relaxation times as a function of particle diameter d: Brownian (dot–dashed line), Néel (dotted line for $K = 15$ kJ m^{-3}; dashed line for $K = 50$ kJ m^{-3}), and the combination (4.3) (solid line with crosses for $K = 15$ kJ m^{-3}; solid line with plusses for $K = 50$ kJ m^{-3}).

5. Comparison with experiments

For the numerical calculations, we take typical values for the ferrofluid APG 933 of FerroTec that is used, among others, in the experiments described in [6]: $M_{\rm sat}^{\rm bulk} = 456$ kA m^{-1}, $\eta = 0.5$ Pa s, $s = 2$ nm, and $f_0 = 10^9$ Hz. Typical values of K lie between 10 and 50 kJ m^{-3} [18, 19]. We furthermore use as input the experimental equilibrium magnetization $M_{\rm eq}(H)$ of APG 933 shown in figure 1 and the magnetic weights of figure 2 obtained with fits to a log-normal distribution or with a regularization method [6].

From previous work [6, 7], we know that single-relaxation time (mono-disperse) models predict the maximum of M_y (resp. of $H_y^{\rm sensor}$) to be located roughly at $\Omega\tau \sim 1$. Furthermore, in the experiments [6] performed with polydisperse ferrofluids for frequencies up to $\Omega \simeq 3000$ rad s^{-1}, mainly the large particles contribute to M_y (resp. to $H_y^{\rm sensor}$), since their magnetic moments are effectively frozen in the particle's crystal lattice. Only these magnetic moments can be pushed out of the direction of the magnetic field by the combined action of thermally induced rotary Brownian motion and deterministic macroscopic flow in the rotating cylinder. Smaller particles can keep their moment aligned with the magnetic field by the Néel process when these particles undergo rotational motion. Finally, the particle diameter that separates Néel behaviour from Brownian behaviour in the size distribution, and that thereby determines how many particles contribute to M_y (resp. to the experimental signal $H_y^{\rm sensor}$), depends sensitively on the anisotropy constant K: the smaller the K, the smaller is the number of Brownian particles according to figure 4, and the smaller is M_y (resp. $H_y^{\rm sensor}$).

The physical picture sketched above is corroborated by figure 5. There we compare the experimentally obtained $H_y^{\rm sensor}(\Omega)$ (stars) as a function of Ω for a representative externally applied field $H_0 = 30$ kA m^{-1} with various model variants that take into account the polydispersity to different degrees. This is done for two different anisotropy constants, namely, $K = 15$ and 50 kJ m^{-3} as representative examples. However, the three uppermost curves refer to single-time relaxation approximations, each with $\tau = 2$ ms [6]: the dotted line with crosses is the result of a strictly monodisperse Debye model, while the lines with diamonds refer to polydisperse models, however with common $\tau_j = \tau = 2$ ms taken in equation (4.1) but different magnetic weights w_j obtained either from a log-normal distribution (full line with full diamonds) or from the regularization method (dashed line with open diamonds). The

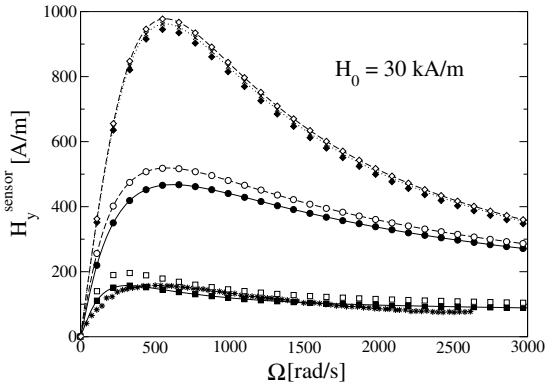

Figure 5. H_y^{sensor} as a function of Ω for $H_0 = 30$ kA m^{-1}. The three uppermost curves refer to single-time relaxation approximations, each with $\tau = 2$ ms: monodisperse Debye model (dotted line with crosses); polydisperse models with common $\tau_j = \tau$ and magnetic weights w_j obtained with a log-normal distribution (full line with full diamonds) and with a regularization method (dashed line with open diamonds). Curves with circles and squares refer to truly polydisperse models (equations (4.1)–(4.3)) with $K = 50$ kJ m^{-3} (circles) and $K = 15$ kJ m^{-3} (squares). Full lines with full symbols were obtained with a log-normal distribution. Dashed lines with open symbols refer to a distribution resulting from the regularization method. In all models, the equilibrium magnetization $M_{\text{eq}}(H)$ was taken to be the experimental one.

equilibrium magnetization $M_{\text{eq}}(H)$ was taken to be the experimental one; the distributions were obtained from this experimental $M_{\text{eq}}(H)$ by the log-normal ansatz (resp. the regularization method). This, first of all, shows that models with only one relaxation time show roughly the same behaviour of $M_y(\Omega)$ irrespective of whether the particle size and magnetic moment distributions are polydisperse or not.

The set of curves with circles and squares in figure 5 refer to truly polydisperse models, equations (4.1)–(4.3), but different anisotropy constants of the magnetic material ($K = 50$ kJ m^{-3} (circles), $K = 15$ kJ m^{-3} (squares)). Again, full lines with full symbols were obtained with a log-normal distribution, while dashed lines with open symbols refer to a distribution resulting from the regularization method. Here, one sees that these two distributions with their magnetic weights displayed in figure 2 yield very similar results, which might not be surprising in view of the fact that both seem to reproduce $M_{\text{eq}}(H)$ adequately.

The largest and most important difference between the curves with diamonds (i.e. the single-time models) and the curves with circles and squares (i.e. the genuine polydisperse models) come from the difference in the anisotropy constants of the magnetic material that governs how many particles contribute efficiently as Brownian particles to the transverse magnetization M_y (resp. to H_y^{sensor}): for smaller K, the magnetic moments of fewer particles, being Brownian particles, may be rotated out of the direction of the magnetic field by the flow in the cylinder.

The curves for $K = 15$ kJ m^{-3} yield roughly the same maximal size H_y^{sensor} as the experiments—they could be fine-tuned even further. But then the location, $\Omega^{\max}(H_0)$, of the maxima for different H_0 is still off from the experimental ones, as shown in figures 6(a) and 7(b). However, the agreement between the predictions of the polydisperse models of equations (4.1)–(4.3) and the experiments concerning the location $\Omega^{\max}(H_0)$ can be improved by allowing the relaxation rates τ_j of the differently sized particles to depend also on the internal field H. To demonstate this, for simplicity we use the form [6]

$$\tau_j^{\gamma}(H) = \tau_j \frac{2\mathcal{L}(\gamma H)}{\gamma H - \mathcal{L}(\gamma H)} \tag{5.1}$$

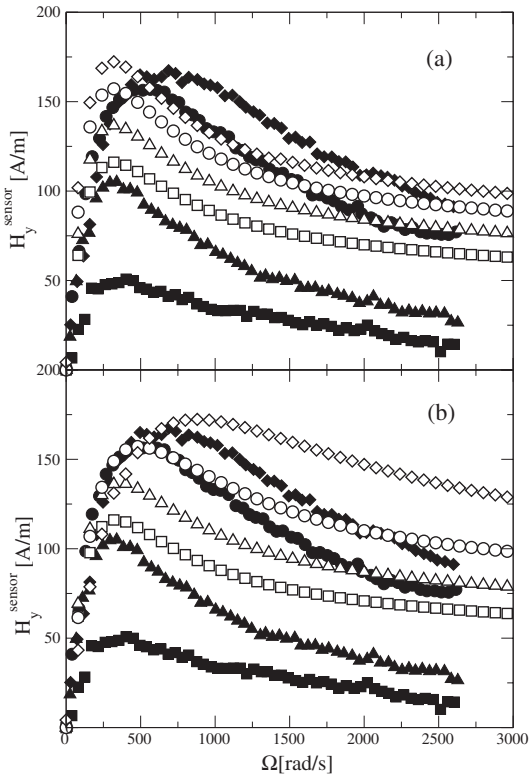

Figure 6. H_y^{sensor} as a function of Ω for $H_0 = 8.6$ kA m^{-1} (squares), 15 kA m^{-1} (triangles), 30 kA m^{-1} (circles), and 60 kA m^{-1} (diamonds). Full symbols denote experimental data. Open symbols refer to the polydisperse model (equations (4.1)–(4.3)) with log-normal distribution and $K = 15$ kJ m^{-3}: in (a) the relaxation times τ_j are independent of H; in (b) they are replaced by $\tau_j^{\gamma}(H)$ (5.1) with $\gamma = 10^{-4}$ m A^{-1}.

with one additional fit parameter γ. Values of about $\gamma \sim 10^{-4}$ m A^{-1} yield maximum locations $\Omega^{\max}(H_0)$ that agree well with the experiments, as can be seen in figures 6(b) and 7(b). This generalization of the model (4.1)–(4.3) leaves the peak value $H_y^{\text{sensor}}(\Omega^{\max})$ almost unchanged, cf figure 7(a).

However, this augmented polydispersive model also reproduces, with fixed values of K and γ, the experimental data only in a small range of Ω and H_0, cf figures 6 and 7.

6. Conclusion

We have compared the predictions of polydisperse models of the magnetization dynamics of ferrofluids with recent experiments measuring the transverse magnetization component M_y of a rotating ferrofluid cylinder. The models use mixtures of mono-disperse ideal paramagnetic gases of differently sized particles. The magnetization dynamics of the models take into account the rigid body rotation of the fluid combined with a simple Debye relaxation of the magnetic moments of each particle with size-dependent Brownian and Néel magnetic relaxation times. Thus, in the absence of flow, each magnetic moment, and with it each sub-magnetization, would be driven independently of the others towards its respective mean

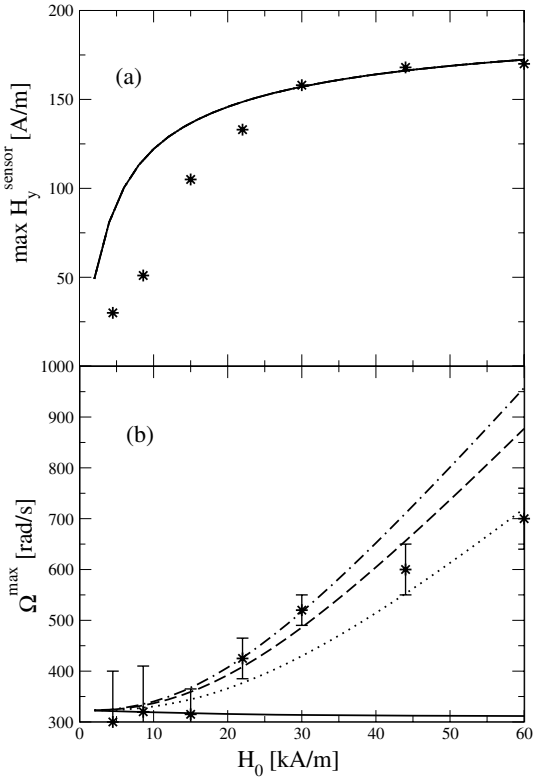

Figure 7. Maximum magnitude max $H_y^{\text{sensor}} = H_y^{\text{sensor}}(\Omega^{\max})$ (a) and location of the maximum $\Omega^{\max}$ (b) as functions of the external field H_0. Stars show experimental data. Lines refer to the results of polydisperse models with a log-normal distribution and $K = 15$ kJ m^{-3}: H-independent relaxation times (solid); H-dependences with $\gamma = 0.8 \times 10^{-4}$ m A^{-1} (dotted), $\gamma = 10^{-4}$ m A^{-1} (dashed), and $\gamma = 1.1 \times 10^{-4}$ m A^{-1} (dot–dashed). In (a), the differences between the lines are too small to be seen.

equilibrium value which, however, depends on the internal magnetic field **H** being collectively generated by all magnetic moments.

The comparison suggests that mainly the large particles contribute to M_y, since their magnetic moments are effectively frozen in the particle's crystal lattice. Only these magnetic moments can be pushed effectively out of the direction of the magnetic field by the combined action of thermally induced rotary Brownian motion and deterministic macroscopic flow in the rotating cylinder. Smaller particles can keep their moment aligned with the magnetic field by the Néel process when these particles undergo rotational motion.

Finally, the particle diameter that separates Néel behaviour from Brownian behaviour in the size distribution, and that thereby determines how many particles contribute to M_y (resp. to the experimental signal H_y^{sensor}), depends quite sensitively on the anisotropy constant K of the magnetic material. K determines how many magnetic moments are 'frozen' or 'blocked' in particles and thus can be rotated by the rigid body flow: the smaller the K, the smaller is the number of Brownian particles with frozen moments, and the smaller is the resulting M_y. Or, vice versa, a large transverse magnetization can be expected in ferrofluids with large anisotropy constants.

An analysis of the rotation rates $\Omega^{\max}(H_0)$ for which M_y is largest indicates that the agreement between experiments and model predictions can be improved by allowing the relaxation rates of the differently sized particles to depend also on the magnetic field H.

Acknowledgments

This work was supported by the Deutsche Forschungsgemeinschaft (DFG) (SFB 277) and by INTAS(03-51-6064).

References

[1] Rosensweig R E 1985 *Ferrohydrodynamics* (Cambridge: Cambridge University Press)
[2] Blums E, Cebers A and Maiorov M M 1997 *Magnetic Fluids* (Berlin: Walter de Gruyter)
[3] Odenbach S 2002 *Magnetoviscous Effects in Ferrofluids* (*Springer Lecture Notes in Physics* vol m71) (Berlin: Springer)
[4] Odenbach S (ed) 2002 *Ferrofluids—Magnetically Controllable Fluids and Their Applications* (*Springer Lecture Notes in Physics* vol 594) (Berlin: Springer)
[5] McTague J P 1969 *J. Chem. Phys.* **51** 133
[6] Embs J P, May S, Wagner C, Kityk A V, Leschhorn A and Lücke M 2006 *Phys. Rev.* E **73** 036302
[7] Leschhorn A and Lücke M 2006 *Z. Phys. Chem.* **220** 219
[8] Shliomis M I 1972 *Sov. Phys.—JETP* **34** 1291
[9] Felderhof B U and Kroh H J 1999 *J. Chem. Phys.* **110** 7403
[10] Felderhof B U 2000 *Phys. Rev.* E **62** 3848
[11] Shliomis M I 2001 *Phys. Rev.* E **64** 060501
[12] Müller H W and Liu M 2001 *Phys. Rev.* E **64** 061405
[13] Embs J, Müller H W, Krill C E, Meyer F, Natter H, Müller H, Wiegand S, Lücke M, Hempelmann R and Knorr K 2001 *Magnetohydrodynamics* **37** 222
[14] Weser T and Stierstadt K 1985 *Z. Phys.* B **59** 253
[15] Leschhorn A and Lücke M 2006 *Z. Phys. Chem.* **220** 89
[16] Embs J, Müller H W, Wagner C, Knorr K and Lücke M 2000 *Phys. Rev.* E **61** R2196
[17] Embs J, Müller H W, Lücke M and Knorr K 2000 *Magnetohydrodynamics* **36** 387
[18] Fannin P C, Preov P A and Charles S W 1999 *J. Phys. D: Appl. Phys.* **32** 1583
[19] Fannin P C 1994 *J. Magn. Magn. Mater.* **136** 49